MHD HEAT TRANSFER IN ELONGATED RECTANGULAR DUCTS FOR LIQUID METAL BLANKETS

Alice Y. Ying and Mark S. Tillack
Department of Mechanical, Aerospace and Nuclear Engineering
University of California, Los Angeles
Los Angeles, CA 90024-1597, USA

ABSTRACT

Laminar heat transfer in self-cooled liquid metal blankets can be enhanced by increasing the aspect ratio of the ducts. To determine the potential benefits of elongated rectangular ducts, numerical simulations of MHD fully-developed flow and developing heat transfer were performed.

Results show that as the aspect ratio increases (i.e., the ratio of the side wall to Hartmann wall length), the peak velocity and side layer flow quantity increase, which leads to enhancement of the average heat transfer coefficient along the side layer. The pressure gradient decreases with increasing elongation, providing an added benefit. However, results of the heat transfer analysis also indicate that the nonuniformity along the heated wall and the peak wall temperature both increase as the aspect ratio increases, due to smaller velocities in the corners and near the interface between the side layer and the core. The net benefit to reactor blanket design is therefore uncertain, because designs are usually constrained by the peak structure temperature. At fixed velocity, elongated ducts always have higher peak temperatures.

However, the reduction in pressure gradient allows the designer to increase the average velocity, which improves thermal performance due to lower bulk temperature rise as well as higher wall heat transfer coefficient. Calculations show that peak temperatures can be reduced relative to the square duct case with lower pressure gradient by optimizing the velocity.

Elongated ducts may suffer from larger pressure stresses due to geometric factors. Thermal stresses are also likely to increase, owing to the increased thermal gradients in the walls. Overall, it is difficult to guarantee that elongation will provide improved performance without a more detailed design analysis.

I. INTRODUCTION

Rectangular ducts with large aspect ratios (ratio of duct width to height) have been proposed in a Soviet blanket concept and for US-Soviet benchmark problems[1]. The pressure gradient, velocity profiles and thermal performance of this "slot duct" geometry are analyzed here to determine its potential net benefits on liquid metal blanket design.

The analysis is based on laminar heat transfer with fully-developed velocity profiles. Previous experimental observations have indicated that if the channels are oriented predominantly in the poloidal direction, then the large toroidal field will estiablish fully developed flow conditions after a few characteristic lengths.[2] The first wall coolant channels have transverse dimensions of a few centimeters, whereas their length is of the order of a few meters. The use of fully developed velocity profiles for heat transfer analysis is thus expected to be appropriate for most practical design purposes. Recent observations[3] indicate that fluctuations could be present near side layers, making the assumption of laminar flow incorrect; however, current understanding of this effect is not sufficient to incorporate into this modeling.

II. VELOCITY PROFILE SOLUTION METHOD

Numerical solutions of fully developed velocity profiles are obtained using the finite element method (FEM) for the geometry shown in Figure 1 (in these cases using $\theta=0$).[4] Velocity profiles are computed for a given pressure gradient, magnetic field strength and direction. The governing nondimensional MHD equations are stated as follows:

$$\frac{dp^*}{dz^*} = \frac{1}{Ha^2}\nabla^{*2} v^* + \left(B_y^* \frac{\partial \phi^*}{\partial x^*} + B_x^* \frac{\partial \phi^*}{\partial y^*}\right) - v^* \qquad (1)$$

$$\frac{\sigma}{\sigma_f}\nabla^{*2}\phi^* - \frac{\sigma}{\sigma_f}\left(B_x^* \frac{\partial v^*}{\partial y^*} - B_y^* \frac{\partial v^*}{\partial x^*}\right) = 0 \qquad (2)$$

Where σ denotes wall or fluid conductivity depending on the location of the element. The unknowns to be solved are the 2-D fully-developed velocity and electric potential profiles, v and ϕ. The nondimensional parameters (those marked with *) are defined using a characteristic scale length, velocity, magnetic field, and fluid conductivity (L_o, v_o, B_o, σ_f):

$$x^* = \frac{x}{L_o} \qquad B^* = \frac{B}{B_o}$$

$$v^* = \frac{v}{v_o} \qquad p^* = \frac{p}{\sigma_f u_o B_o^2 L_o}$$

$$J^* = \frac{J}{\sigma_f u_o B_o} \qquad \phi^* = \frac{\phi}{u_o L_o B_o}$$

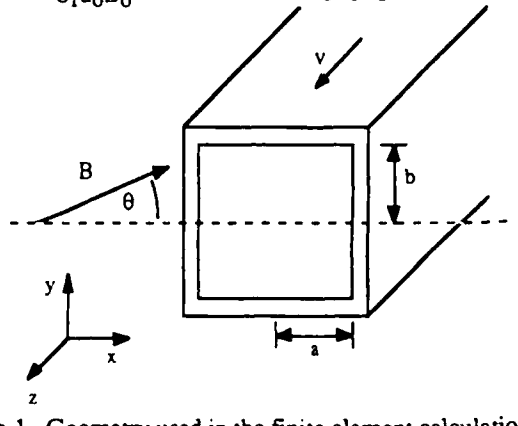

Figure 1. Geometry used in the finite element calculation

The Hartmann number is given by $Ha=L_oB\sqrt{\sigma_f/\mu}$, where μ is the fluid viscosity. The boundary equations include zero velocity at the wall, zero current out of the duct, and pressure gradient set to unity ($\hat{n}$ is the normal to the wall):

$$v = 0 \quad \text{at} \quad x = \pm 1 \text{ or } y = \pm \frac{b}{a}$$

$$\nabla\phi \cdot \hat{n} = 0 \text{ at the surface}$$

$$\frac{dp^*}{dz^*} = 1 \tag{3}$$

The duct walls are directly modeled to determine the electric potential and currents. Continuity of the potential and current is imposed at the interface between the fluid and the walls. The duct can be elongated in the direction either parallel or perpendicular to the magnetic field.

III. MHD CODE VALIDATION

A. Grid Dependence

The accuracy of the solution depends on proper selection of element sizes. In these analyses, the grid is made spatially nonuniform to concentrate more nodes in the regions near the walls and the interfacial region between the boundary layer and the fluid core, where the variation in velocity is highest. (The thickness of this region increases as the aspect ratio increases due mainly to the fact that the MHD boundary layer thickness is proportional to the dimension parallel to the field line). The calculations were performed by reducing the element size until the solution no longer depended on the element size.

For a square duct with Ha=5000, an element size in the side layer region of 0.25% of the duct width gives the correct solution. For this case, the side layer thickness is about 1.4% of the duct size. Thus, several elements within the side layer are needed. For aspect ratio different than 1, a rectangular element with element aspect ratio around 2 to 3 was used successfully. Fine elements were used to cover the entire boundary layer region.

B. Comparison of Pressure Gradient and Fraction of Flow in the Core with the Circuit Network Analogy

The pressure gradient and fraction of flow quantity in the core obatined from finite element solutions for a conducting duct were compared with analytical solutions obtained from Tillack[5]. The analytical solutions were obtained for general rectangular ducts using an electric circuit network analogy, including consideration of the influence of side layers and Hartmann layers. The final expression for the pressure gradient in a conducting rectangular duct is written as:

$$\nabla^* p^* = \frac{1}{\frac{a/b}{3}\frac{Ha^{1/2}}{1+\Phi_{sw}Ha^{1/2}} + \frac{\Phi_{Hw}+1}{\Phi_{Hw}+\frac{1}{Ha}}} \tag{4}$$

where p is normalized as shown above, using an average velocity equal to 1. Here, the Hartmann number is defined in terms of the channel half-width along the magnetic field lines, "a". The side wall conductance ratio and Hartmann wall conductance ratio are also defined in terms of "a":

$$\Phi_{sw} = \frac{\sigma_{sw}\, t_{sw}}{\sigma_f\, a}$$

$$\Phi_{Hw} = \frac{\sigma_{Hw}\, t_{Hw}}{\sigma_f\, a} \tag{5}$$

The aspect ratio is defined as $\varepsilon=a/b$, where "a" is the channel half-width parallel to the field line and "b" is the channel half-width perpendicular to the field line, "t" is the wall thickness, and the subscripts sw and Hw refer to the Hartmann wall and side wall, respectively.

For the presentation of results, an attempt was made to maintain most of the conditions constant while changing only one parameter at a time. This can be difficult, because the Hartmann number, wall conductance ratio, and aspect ratio all change as the duct dimensions are varied. To provide the most meaningful results, the Hartmann number is defined in terms of the dimension which is fixed. When $\varepsilon<1$, "a" is held constant and "b" is increased. In this case, $Ha^{(a)}$=constant, where $Ha^{(a)}=aB\sqrt{\sigma/\mu}$. When $\varepsilon>1$, "b" is held constant and "a" is increased. In this case, $Ha^{(b)}$=constant, where $Ha^{(b)}=bB\sqrt{\sigma/\mu}$. For all cases, the wall thickness (t) and magnetic field strength (B) are held constant.

The pressure gradient values obtained from the finite element results are shown in Fig. 2 and compared with the results calculated from Eq. 4 and also with Walker's solution.[6] For all cases, Ha=5000, t=0.05 and the wall and fluid conductivities are equal ($\sigma_w=\sigma_f$). Excellent agreement is found under these conditions over a range of channel aspect ratios. The results indicate that the pressure gradient decreases as the aspect ratio increases. This is partly due to the decrease in effective wall conductance ratio as the parallel dimension increases; however, the pressure drop decreases more rapidly than the wall conductance ratio. The pressure drop is reduced by a factor of 20 as the aspect ratio changes from 1 to 10. The pressure gradient changes only slightly for aspect ratios less than 1 (obtained by increasing "b").

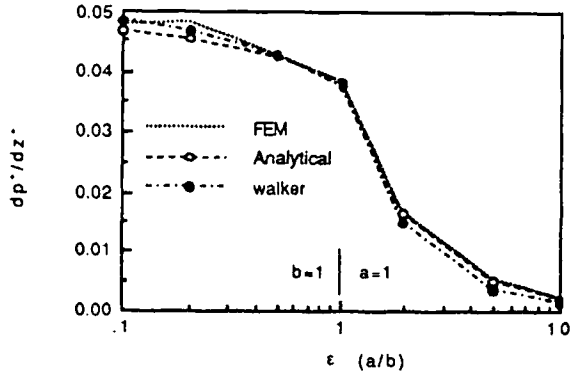

Fig. 2. Comparison of pressure gradient using FEM solution, circuit network analogy, and Walker's solution

The flow quantity in side layers is particularly important because of the large potential effect on heat transfer coefficients and peak wall temperatures. Parameters which influence the flow quantity in the side layer (or core) are the aspect ratio, the Hartmann number, and the wall conductance ratio. Analytical solutions for the fraction of flow in the side layer were obtained using the electric circuit network analogy[5] by integrating the normal component of Ohm's law through the side layer:

$$\int (J/\sigma_f) \cdot dy = \int (v \times B) \cdot dy - \int (\nabla\phi) \cdot dy \qquad (6)$$

The final expression for the fraction of flow in the core for general rectangular duct with different wall conductance ratios was expressed as:

$$f_c = \frac{\dfrac{\Phi_{Hw} + 1}{\Phi_{Hw} + \dfrac{1}{Ha}}}{\dfrac{a/b}{3\Phi_{sw}} \dfrac{1}{1 + \dfrac{1}{\Phi_{sw} Ha^{1/2}}} + \dfrac{\Phi_{Hw} + 1}{\Phi_{Hw} + \dfrac{1}{Ha}}} \qquad (7)$$

The fraction of flow in the side layers is simply written as:

$$f_{sl} = 1 - f_c \qquad (8)$$

The above expressions were compared with FEM results for different aspect ratios and tabulated in Table 1. The core velocity is equivalent to the fraction of flow in the core if the average velocity is set equal to 1. Excellent agreement is found between the analytical expression and FEM solutions.

Table 1. Core flow fraction using Eq. 7 compared with 2-D numerical solutions. (Ha=5000, t=0.05, $\sigma_f=\sigma_{sw}$)

a	b	f_c (Eq. 7)	f_c (FEM solution)
1	10	0.976	0.977
1	5	0.953	0.955
1	2	0.890	0.886
1	1	0.810	0.795
2	1	0.682	0.681
5	1	0.496	0.494
10	1	0.363	0.352

C. Comparison of Velocity Profiles with Hunt's Analytic Solution

An analytic solution for MHD velocity profiles in rectangular ducts was obtained by J.C.R. Hunt[2]. That solution treats ducts with perfectly conducting walls perpendicular to the field and thin walls of arbitrary conductivity parallel to the field. The velocity profiles obtained from FEM calculations were compared with Hunt's solutions for different Hartmann numbers and Φ_{sw}=0.07. Excellent agreement is found under these conditions (see Fig. 3).

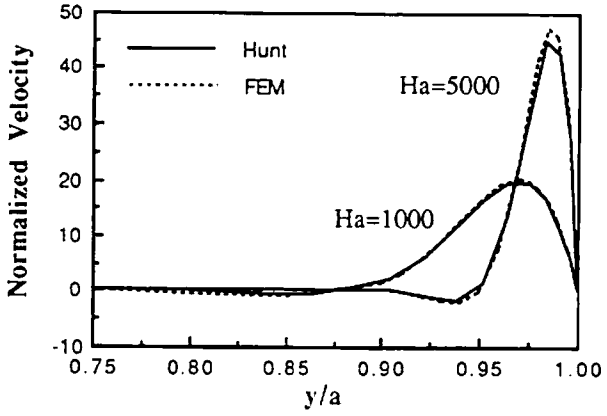

Fig. 3. Comparison of finite element results with Hunt[2]

IV. VELOCITY PROFILE RESULTS AND DISCUSSION

Figure 4 shows an example velocity profile in 1/4 of a duct with Ha=5,000, Φ=0.05, and ε=1 (and a nonuniform grid). A clear side layer velocity is found in the wall parallel to the field line and a dip in velocity is observed at the interface of the MHD boundary layer and core. In the following, for simplicity, velocity profiles are compared by examining the profiles at the centerline of the duct (x=0). The 2-D behavior is generally similar to Figure 4.

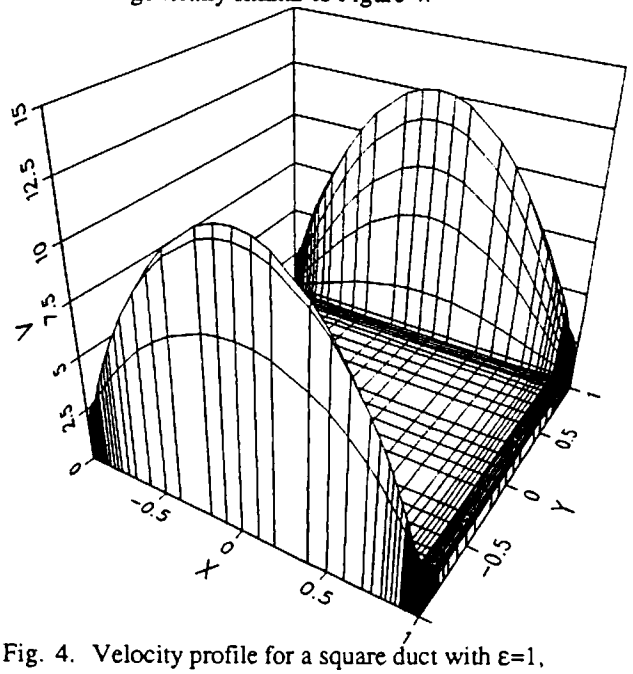

Fig. 4. Velocity profile for a square duct with ε=1, Ha=5,000, and Φ=0.05

A. The case with ε>1

Midplane velocity profiles for a rectangular duct with aspect ratios between 1 and 10 (elongated along the direction of the magnetic field) are shown in Figure 5. The aspect

ratio is increased by increasing "a" while keeping "b" fixed. In all cases, $Ha^{(b)}$=5000.

For these slot geometries with ε>1, the calculations show that the MHD boundary layer thickness increases as the aspect ratio increases. The side layer thickness increases together with the channel half-width parallel to the field line, according to the approximate scaling:

$$\delta sl \sim \frac{a}{\sqrt{Ha}} \tag{9}$$

The flow quantity in the side layer also increases, and therefore the core velocity decreases (see Table 1).

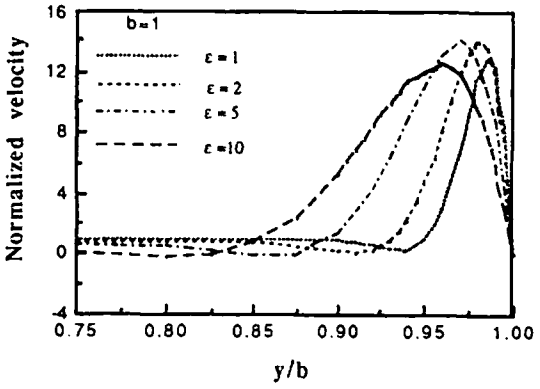

Fig. 5. Mid-plane side layer velocity profiles for ε>1

B. The case with ε<1

The midplane side layer velocity profiles for ducts with aspect ratio ε<1 are shown in Figure 6. The aspect ratio is decreased by increasing "b" while keeping "a" fixed. In all cases, $Ha^{(a)}$=5000. The results indicate that the MHD side layer thickness normalized to "a" stays about the same for these ducts. The peak velocity and fraction of flow quantity in the core increase slightly as ε decreases.

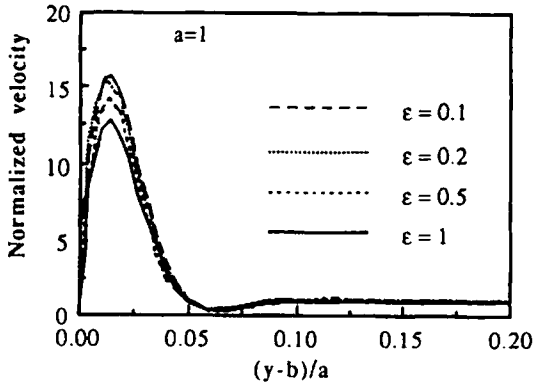

Fig. 6. Mid-plane side layer velocity profiles for ε<1

V. HEAT TRANSFER ANALYSIS

The velocity profiles obtained above were used as input to a three-dimensional finite difference heat transfer code. The code solves the energy equation for the temperature field (T):

$$v \frac{\partial T}{\partial z} = \alpha \nabla^2 T \tag{10}$$

where α is the thermal diffusivity and z is the distance downstream. To account for the sharp velocity gradient close to the side wall, a nonuniform grid with a finer mesh in the side layer was used in the calculation. A uniform heat flux, q, is applied to one wall adjacent to a side layer, starting at z=0. To quantitatively determine the benefit in heat transfer from the use of slot ducts, the bulk temperature rise is kept constant for the different cases studied. The bulk temperature, T_b, is given by:

$$T_b = \frac{\int T\, v\, dx\, dy}{\int v\, dx\, dy} \tag{11}$$

In the following, results are presented in relation to the square duct case, ε=1. This case was analyzed first, and results are shown in Figure 7 as a function of the Fourier number, which measures distance downstream:

$$Fo = \frac{\alpha z}{(vb^2)3} \tag{12}$$

The figure shows the average temperature along the side wall, T_s, the peak wall temperature, T_p, and the bulk temperature rise due to the surface heating, T_b. (In a reactor, the bulk temperature rise due to volumetric heating can be 5–10 times as high as due to surface heating). Temperatures are normalized to the heat flux. In this way, the inverse is related to the Nusselt number, e.g.,

$$\frac{T_s - T_b}{\frac{q''b}{k}} = \frac{2}{Nu_s} \tag{13}$$

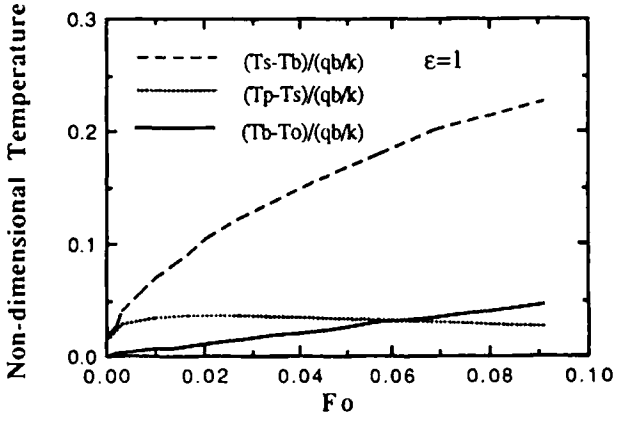

Fig. 7. Wall average and peak temperatures for the case ε=1

where k is the thermal conductivity, h is the heat transfer coefficient, and the Nusselt number is defined by:

$$Nu = \frac{2bh}{k} \tag{14}$$

For this geometry, the average fully-developed Nusselt number approaches ~8. The peak-to-average temperature is seen to be relatively small for the case ε=1, except very close to the inlet. As shown later, the peaking factor increases substantially as the aspect ratio increases.

A. The case with ε>1

For ε>1, the duct is elongated along the magnetic field direction. As the duct is elongated, the total heating and the total mass flow rate increase linearly; the average velocity is maintained constant. This approximates a reactor blanket duct which maintains a constant depth (b).

As the aspect ratio increases, the average side wall temperature decreases. This is expected, because the flow quantity in the side layer has increased. Fig. 8 shows the ratio of the average side wall temperature (minus the fluid bulk temperature) to the average side wall temperature with ε=1.

While the average side wall temperature decreases slightly, the peak-to-average temperature increases substantially. Figure 9 indicates the magnitude of this effect by plotting the peaking factor P as a function of Fourier number for aspect ratios between 1 and 10, where P is given by:

$$P = \frac{(T_p - T_s)_\varepsilon}{(T_p - T_s)_1} \tag{15}$$

T_p is the peak temperature and T_s is the average temperature along the side wall. The enhancement in the average temperature saturates after ε~2, whereas the peak-to-average continues to increase with increasing ε.

The net effect is always an increase in the peak temperature over the case with ε=1 (for fixed average velocity). Figures 7–9 can be used to compute this, since:

$$\frac{(T_p-T_b)_\varepsilon}{\frac{qb}{k}} = \frac{(T_p-T_s)_\varepsilon}{(T_p-T_s)_1}\,\frac{(T_p-T_s)_1}{\frac{qb}{k}} + \frac{(T_s-T_b)_\varepsilon}{(T_s-T_b)_1}\,\frac{(T_s-T_b)_1}{\frac{qb}{k}} \tag{16}$$

In the worst case (ε=10), a factor of 10 additional peaking will reduce the local Nusselt number at the hot spot by more than half as compared with ε=1 (Fig. 7), while the reduced average wall temperature will result in less than 25% increase in Nu. Besides the effect on local temperature, a nonuniform temperature profile will result in higher thermal stresses and geometric deformation, which must be factored into any design comparison.

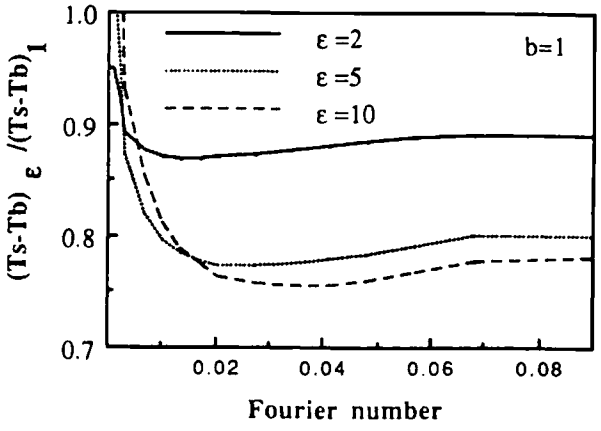

Fig. 8. Average side wall temperature for ε>1

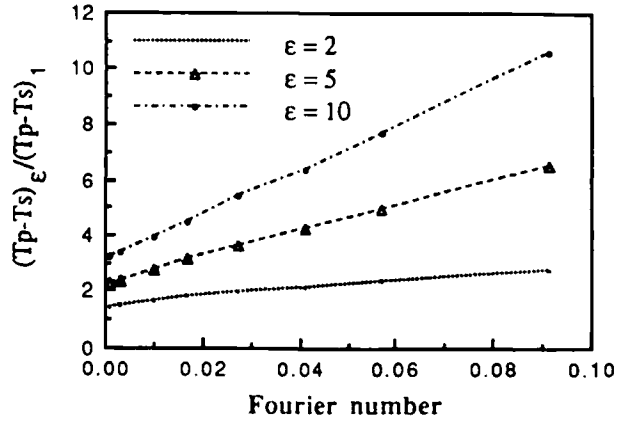

Fig. 9. Side wall temperature peaking factor for ε>1

B. The case with ε<1

For ε<1, the duct is elongated perpendicular to the field. This serves to increase the depth of the blanket. Since "a" is constant, the total heating rate is constant.

The average side layer temperature and peaking factor are plotted in Figures 10 and 11 as a function of Fo for ε<1. The results indicate that the average side layer temperature increases slightly compared with ε=1, leading to a lower average heat transfer coefficient on the side wall. The peak-to-average temperature ratio increases slightly in this case also, and appears to saturate at a low value of ε. Both average and peak temperatures are always higher in this case. This is to be expected due to the larger depth of the duct.

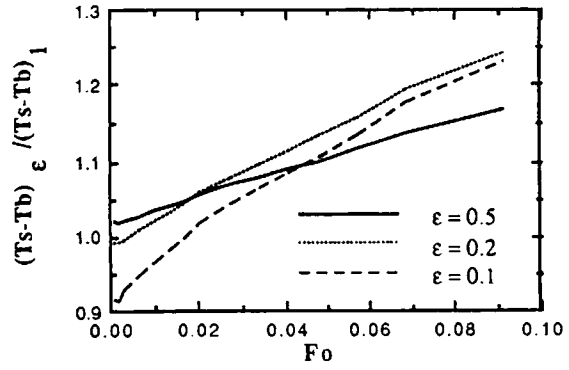

Fig. 10. Average side wall temperature vs. Fo for ε<1

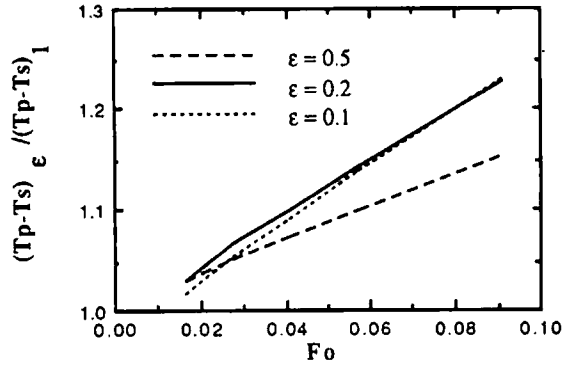

Fig. 11. Side wall peaking factor vs. Fo for ε<1

VI. SUMMARY AND ASSESSMENT

Changes in the dimensions of liquid metal blanket ducts have large and complex effects on the pressure gradient, velocity profiles, and heat transfer. The net impact on the attractiveness of designs depends on the design constraints; however, some general observations are possible.

Under conditions of fixed velocity, the average side wall temperature is generally lower and the peak temperature is higher with elongated ducts as compared with a square channel. Since designs are usually constrained by the peak temperature, the advantage from elongated ducts is dubious.

However, a large decrease in pressure gradient should be counted in favor of ducts with high aspect ratio; the pressure gradient decreases more than linearly. The pressure gradient reduction can more than compensate the effect on peak temperatures. To demonstrate this, Fig. 12 shows the peak temperatures at ε=10 compared with ε=1. In this comparison, the velocity was increased to take advantage of the reduced pressure gradient. As the velocity is raised, both bulk temperature rise as well as wall temperature rise decrease. As seen in the figure, an increase by a factor of 3 in the velocity compensates for the degraded local heat transfer. In this case (see Fig. 2), the pressure gradient is still 7 times lower than for the square duct. This lower pressure gradient may be necessary to maintain resonable pressure stresses, depending on the design details (for example, designs have been proposed using stiffening rods[1] which might partially relieve the problem with pressure stresses in elongated ducts).

Overall, the advantages of elongated ducts are not universal, and depend on a design optimization which includes consideration of the temperature profiles, pressure gradient, pressure stresses, thermal stresses, and design constraints. More detailed analysis will be needed to fully resolve this issue.

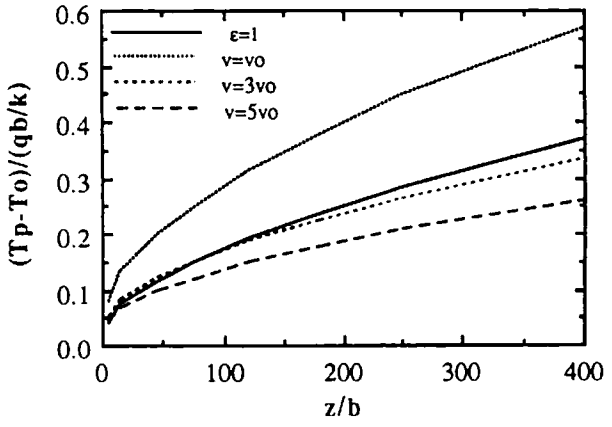

Fig. 12. Comparison of peak temperature vs. distance downstream for ducts with ε=1 and ε=10.

ACKNOWEDGEMENTS

This work was performed under U.S. Department of Energy Contract DE-FG03-ER8652123.

REFERENCES

1. Proceedings of the USSR/US Exchange II.5, "Workshop on Comparison of Liquid Metal Blanket Approaches and Experiments," November 1989.

2. J. C. R. Hunt, "Magnetohydrodynamic Flow in Rectangular Ducts," J. Fluid Mech., Vol. 21, part 4, pp. 577-590 (1965).

3. C. B. Reed and B. F. Picologlou, "Sidewall Flow Instabilities in Liquid Metal MHD Flow Under Blanket Relevant Conditions," Fusion Technology 15(2), March 1989, pp. 705-715.

4. M. Tillack, A. Ying, and H. Hashizume, "The Effect of Magnetic Field Alignment on Heat Transfer in Liquid Metal Blanket Channels," UCLA-FNT-024, March 23, 1989.

5. M. S. Tillack, MHD Flow in Rectangular Ducts – Design Equations for Pressure Drop and Flow Quantity, UCLA-FNT-41, July 1990

6. J. S. Walker, "Magnetohydrodynamic Flows in Rectangular Ducts with Thin Conducting Walls," Journal de Mecanique, vol. 20, no. 1, pp. 79-112, (1981).